JOURNAL OF MATERIALS SCIENCE **39** (2004) 5103–5110

Phase transformations in nanocrystals

J. Z. JIANG
Laboratory of New-Structured Materials, Department of Materials Science and Engineering, Zhejiang University, Hangzhou 310027, People's Republic of China; Department of Physics, Building 307, Technical University of Denmark, Lyngby D-2800, Denmark
E-mail: jiangjz@zju.edu.cn; jiang@fysik.dtu.dk

Recent development of pressure-induced phase transformations in nanocrystals is reported. A thermodynamic theory is presented and three components: the ratio of volume collapses, the surface energy differences, and the internal energy differences, governing the change of transition pressure in nanocrystals were uncovered. They can be used to explain the results reported in the literature and to identify the main factor to the change of the transition pressure in nanocrystals. We demonstrated that the grain-size effect on the structural stability in nanocrystals with respect to transition pressure can be of either sign, depending on the system under investigation.

1. Introduction

Nanocrystals, consisting of small crystallites of diameter 1–100 nm, often have novel physical and chemical properties, differing from those of the corresponding bulk materials [1]. For example, nanometer-sized semiconductors exhibit particle size dependence of electronic and optical properties, making them potential candidates for applications involving tunability of electronic or optical properties [2, 3]. The issue of the effects of crystallite size on structural stability in these nanocrystals is of considerable interest from a fundamental viewpoint, and also with respect to the applicability of these materials. How will the relative stability of different possible solid structures change for nanocrystals with respect to bulk materials? One way to answer this question is to use pressure to force nanostructured materials to convert from one solid structure to another. Recently, Tolbert *et al*. [4–6] reported their studies on Si, CdSe and CdS nanocrystals, and found that the smaller the crystallite, the higher the transformation pressure. They explained the increase in transition pressure for the nanocrystals in terms of surface-energy differences between the phases involved. Qadri *et al*. [7] reported that the effect of reduced grain size in PbS nanocrystals is to elevate the transition pressure, while the compressibility increases with decreasing grain size. An enhancement of transition pressure in nanocrystals ZnO [8], ZnS [9], PbS [10] compared with corresponding bulk material was also observed. However, Jiang *et al*. [11] reported that for nanometer-sized γ-Fe_2O_3 particles the phase transition pressure (from γ-Fe_2O_3 to α-Fe_2O_3) is much lower than that for bulk material. They suggested that the larger volume change upon transition in the nanocrystals is the main factor. A reduction of transition pressure was also reported in nanocrystals TiO_2 for the rutile-to-α-PbO_2 transition [12]. Very recently, Rekhi *et al*. [13] also found that fluorite-type CeO_2 undergoes a phase transition to an orthorhombic $PbCl_2$-type structure at pressure around 26.5 GPa for nanocrystalline CeO_2, which is less than 32 GPa for bulk CeO_2. In the first part of this paper we summarize results obtained from an ongoing systematic study of the phase stability in nanocrystals. The nature of the change of transition pressure in nanocrystals as compared with the corresponding bulk material is addressed from thermodynamic consideration.

2. Experimental

All nanocrystalline materials except γ-Fe_2O_3 were produced by ball milling using a Fritsch Pulverisette ball mill with tungsten carbide or stainless steel vials and balls. The starting material consisted of high-purity (99.9%) powders of about 10 μm particle size. After ball milling for typically 80 h, the average grain size was about 10 nm. Nanocrystalline γ-Fe_2O_3 was obtained by oxidation of Fe_3O_4 particles prepared by coprecipitation. The nanocrystalline materials were characterized by X-ray diffraction (XRD) and transmission electron microscopy (TEM).

The techniques, which we used to monitor phase transformations, are *in-situ* high-pressure X-ray powder diffraction using synchrotron radiation, *in-situ* high-pressure electrical resistance and optical measurements. *In-situ* high-pressure electrical resistance measurements at ambient temperature were carried with a 1200-ton multi-anvil apparatus using 10 and 7 mm edge length octahedral pressure cells without pressure transmitting medium. Copper foils were used as electrodes to measure the dc resistance across of sample disk of approximate dimensions 0.9 mm diameter and 0.5 mm thick. Resistance measurements were made on increasing pressure using a previous determined pressure calibration that is based on several pressure standards. High-pressure optical measurements were performed in a Mao-Bell type diamond anvil cell with 0.4 mm flat tables. The powder samples were directly compressed in a 0.4 mm hole of a nickel gasket without pressure

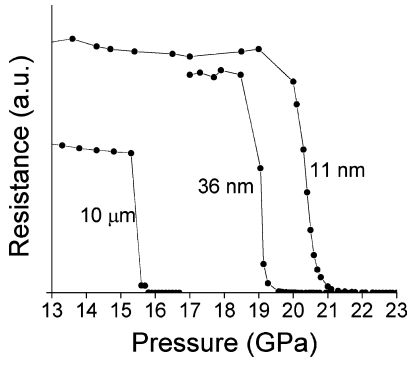

Figure 1 In-situ high-pressure electrical resistance for ZnS materials with average grain sizes of 10 μm, 36 nm, and 11 nm at ambient temperature.

transmitting medium. The pressure was measured by using small ruby chips placed on the top diamond. Low and high-pressure phases show different contrast in many cases, so that the phase boundary is well defined. By increasing the applied load to the diamonds the limit of the high-pressure phase moves in the pressure gradient and the transition pressure was accurately measured when the phase boundary was just crossing a ruby chip. *In-situ* high-pressure X-ray diffraction measurements were recorded at Hasylab in Hamburg, Germany, using synchrotron radiation energy-dispersive method in the 10–70 keV energy range. High pressures up to 50 GPa were obtained in a Syassen-Holzapfel type diamond anvil cell [14]. The powder sample and a small ruby chip were enclosed in a hole of diameter 200 μm in an inconel gasket. A 16:3:1 methanol:ethanol:water solution or silicon oil was used as a pressure transmitting medium. The actual pressure was determined from the wavelength shift of the ruby line using the non-linear pressure scale of Mao *et al*. [15].

3. Nanocrystals

3.1. Enhanced transition pressure

An enhancement in the transition pressure with decreasing grain size has been observed for a number of systems. The first experimental report is on nanometer-sized CdSe system from Alivisatos' group [4]. They used *in-situ* high-pressure X-ray powder diffraction and observed an enhancement of transition pressure for zincblende (B3)-to-rocksalt (NaCl or B1) phase transformation in CdSe nanocrystals as compared with bulk material. Recently, we have studied the zincblende (B3)-to-rocksalt (NaCl or B1) phase transformation in ZnS nanocrystals by three techniques mentioned in the experimental section. Fig. 1 shows high-pressure *in-situ* electrical resistance for ZnS materials with average grain sizes of 10 μm, 36 nm, and 11 nm. It is clearly seen that the semiconductor-to-metal transition occurs at pressures of approximately 19.0 $\pm$ 0.4 GPa and 20.5 $\pm$ 0.6 GPa for the 36 nm and 11 nm ZnS, respectively, whereas for the 10 μm ZnS it occurs at approximately 15.6 $\pm$ 0.3 GPa. The data show that the semiconductor-to-metal transition pressure strongly depends on the grain size of ZnS crystals. The smaller the crystal, the higher the transition pressure. These results were beautifully confirmed by high-pressure optical observations for bulk ZnS and the 11 nm nanocrystals, as shown in Fig. 2. It is found that the semiconductor-to-metal transition for the 11 nm ZnS (Fig. 2b) appears at around 21.8 $\pm$ 0.6 GPa while the 10 μm sample (Fig. 2a) has a transition at around 16.0 $\pm$ 0.5 GPa, in good agreement with the data obtained in Fig. 1. The pressured-induced changes of electronic and optical properties in ZnS are reflected by a structural change, which can be monitored by *in-situ* high-pressure synchrotron radiation X-ray powder diffraction measurements. Fig. 3 exemplifies diffraction patterns of 10 μm and 11 nm ZnS at pressures ranging

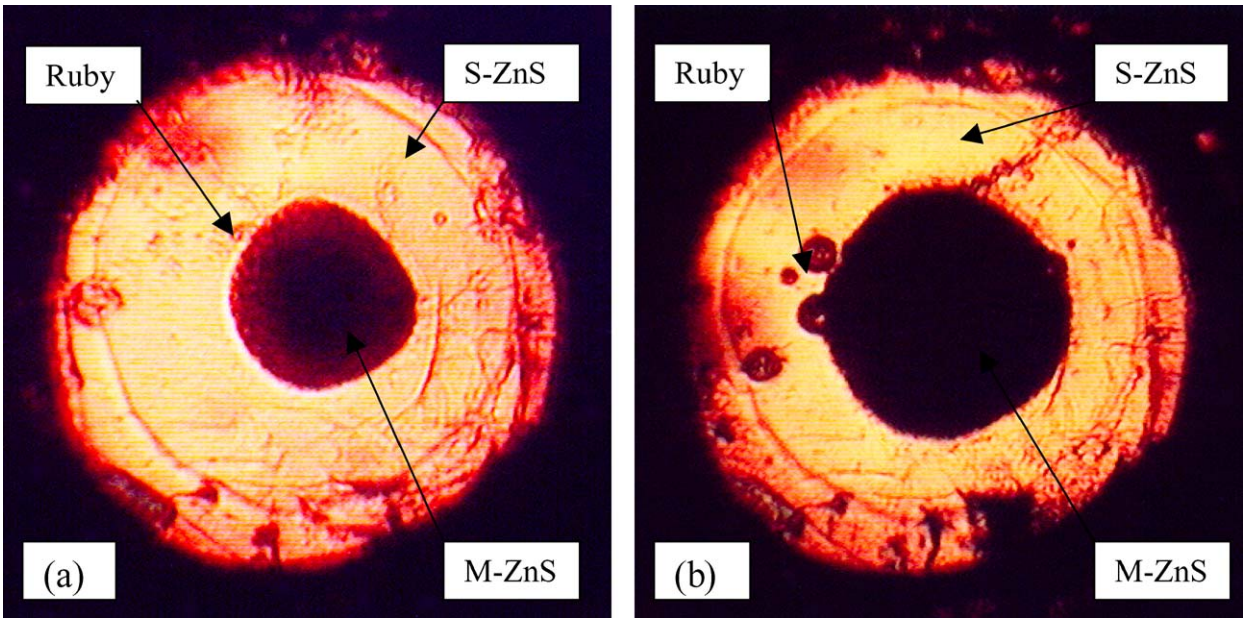

Figure 2 In-situ high-pressure optical micrographs of the semiconductor-to-metal transitions for ZnS materials with average grain sizes of 10 μm (a) and 11 nm (b). The high-pressure metallic phase (M-ZnS) is opaque compared with the low-pressure semiconducting phase (S-ZnS), so that the phase boundary is quite well defined. The transition pressures were determined to be 21.8 $\pm$ 0.6 and 16.0 $\pm$ 0.5 GPa for 11 nm and 10 μm ZnS samples, respectively.

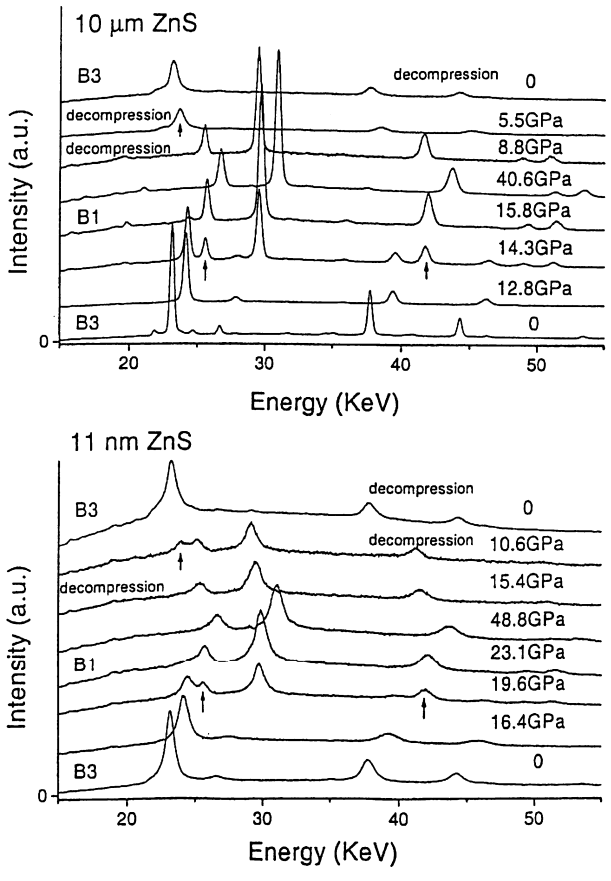

Figure 3 Examples of *in-situ* high-pressure synchrotron radiation X-ray powder diffraction patterns at room temperature with increasing and decreasing pressures for 10 μm and 11 nm ZnS. B3 and B1 are the low- and high-pressure phases.

from 0 to about 50 GPa at room temperature, with increasing and decreasing pressures. In both samples, the low-pressure semiconductor phase has a B3 structure while the high-pressure metal phase has a NaCl-type (B1) structure. For the 10 μm sample, the B3-to-B1 phase transition observed starts approximately 14 GPa and ends at approximately 16 GPa. At the transition ($P_B \sim 15 \pm 1$ GPa), the volume collapse is found to be $[V_B(B3, P_B) - V_B(B1, P_B)]/V_B(B3, P_B) = 17 \pm 1\%$. The single high-pressure B1 phase remains up to about 50 GPa. In decompression, the B1 phase is stable down to 8.8 GPa and a B1-to-B3 phase transition occurs at approximately 6 GPa. For the 11 nm ZnS, it is clearly seen that only the B3 phase is detected up to 16.4 GPa and the B3-to-B1 phase transition is observed, starting approximately 19 GPa and ending at a pressure below 23.1 GPa. At the transition ($P_n \sim 21 \pm 1$ GPa), the volume collapse is found to be $[V_n(B3, P_n) - V_n(B1, P_n)]/V_n(B3, P_n) = 17.5 \pm 1\%$. The single high-pressure B1 phase remains up to about 50 GPa. In decompression, the B1 phase is stable down to 15.4 GPa and the B1-to-B3 phase transition already occurs at approximately 10.6 GPa. Bulk modulus, B_o, and its pressure derivative, B'_o, of B3 phase is estimated from the Birch-Murnaghan equation of state [16] in a pressure range from 0 to 9 GPa. They are $B_o = 72 \pm 7$ GPa and $B'_o = 9 \pm 3$ for 11 nm ZnS and $B_o = 68 \pm 3$ GPa and $B'_o = 7 \pm 1$ for 10 μm ZnS. In contrast to PbS [7], no obvious difference in compressibility for ZnS samples with various grain sizes was detected within experimental uncertainty. It should be mentioned that the semiconductor-to-metal transitions in a few II–VI compounds, including ZnS, are used to make up the fixed-point static pressure calibration curve as a function of hydraulic oil pressure in the pressure range from 1 to 25 GPa for the multianvil high-pressure apparatus. This instrument has been used in many disciplines, e.g., geoscience, materials science, and physics [17], due to its advantages of larger sample volume and long high temperature stability despite the relative low maximum achievable pressure as compared with the laser-heated diamond anvil cell. On the basis of the results obtained for the ZnS samples, therefore, it can be concluded that the dangers of using the transition pressures of the II–VI compounds as pressure calibrators without a detailed knowledge of their grain-size effects on the transition pressures cannot be overstressed.

At ambient temperature, bulk PbS has a phase transformation at 2.2 GPa from a NaCl-type structure (B1) to a black phosphorus-type orthorhombic structure (B16) [18]. Qadri *et al.* [7] reported synchrotron radiation energy-dispersive high-pressure X-ray powder diffraction measurements of PbS with three different grain sizes. They found that onset and completion pressures of the B1-to-B16 transition increase with decreasing grain size. However, due to small grain sizes and the fact that B16 is a distorted cubic B1 phase, the broad diffraction lines of B1 and B16 phases strongly overlapped. Consequently, the determination of the transition pressure for the B1-to-B16 transformation in PbS using X-ray powder diffraction technique becomes questionable. Therefore, we reexamined the grain-size effect on the phase transition in PbS using *in-situ* high-pressure conductivity measurements [10]. We found that the transition is associated with a sharp increase in resistivity by three orders of magnitude [10]. This resistivity change takes place in the pressure range 2.4–3.8 GPa for bulk PbS material. For 8 ± 1 nm PbS nanocrystals corresponding resistivity change takes place in the range 5–7.6 GPa. The mean transition pressure is estimated to 3.1 ± 0.7 GPa for bulk PbS and 6.3 ± 1.7 GPa for the nanocrystalline material. These results have been confirmed by *in-situ* high-pressure X-ray diffraction measurements [7, 10]. In the PbS system, it also reveals that the smaller the crystal, the higher the transition pressure.

The wurtzite (B4)-to-rocksalt (NaCl or B1) phase transformation in ZnO nanocrystals has also been investigated by *in-situ* high-pressure X-ray powder diffraction, conductivity and optical measurements [8]. The results of the high pressure behaviour of bulk ZnO obtained are in good agreement with those reported in previous studies [19–26]. A B4-to-B1 transition is observed, starting at approximately 9 GPa and ending at approximately 11 GPa, with a volume collapse of approximately 16.4%. The high pressure B1 phase stables up to 52.5 GPa. Upon decompression, a large fraction of the B1 high pressure phase is retained when the pressure is released, indicating a substantial phase hysteresis. Fig. 4 shows X-ray powder diffraction patterns at various pressures for ZnO nanocrystals. The

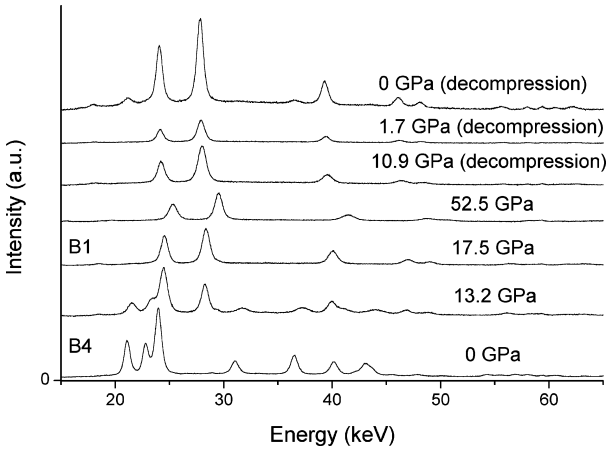

Figure 4 Examples of *in-situ* high pressure synchrotron radiation X-ray powder diffraction patterns at room temperature with increasing and decreasing pressures for 12 nm ZnO nanocrystals. It indicates the co-existence of the wurtzite and rocksalt phases at 13.2 GPa. The high pressure B1 phase is stable up to 52.5 GPa. Upon decompression, single B1 phase was found down to 1.7 GPa and it dominates the pattern recorded at 0 GPa.

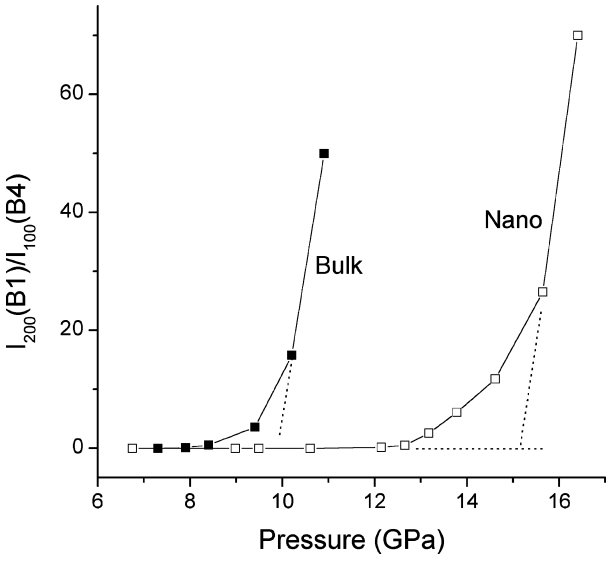

Figure 5 Intensity ratio $I_{200}(B1)/I_{100}(B4)$ vs. pressure for ZnO. Filled and open squares denote bulk and nanocrystals, respectively. The 200 line of the B1 phase and the 100 line of the B4 phase have no counterparts in the B4 and B1 phases, respectively. Thus, the intensity ratio, $I_{200}(B1)/I_{100}(B4)$, approaches infinity at the final stage of the transformation.

B4-to-B1 transition is also observed in nanocrystals. The transition is illustrated by the intensity ratio of the 200 (B1) to 100 (B4) peaks as a function of pressure, as shown in Fig. 5. Using the extrapolation procedure the transition pressure is estimated to be 15.1 GPa for the nanocrystal ZnO and 9.9 GPa for the bulk ZnO. There is a 50% enhancement of the transition pressure in the nanocrystal ZnO as compared with the bulk material. Fig. 6 shows the pressure dependence of the relative volume. The volume collapse by the transition was approximately 15.6% in ZnO nanocrystals. It was suggested that the high-pressure B1 phase could be metallic with respect to the semiconductor low-pressure B4 phase [27]. Thus, we performed *in-situ* high-pressure electrical resistance measurements for both bulk and 12 nm ZnO materials. No semiconductor-to-metal transition

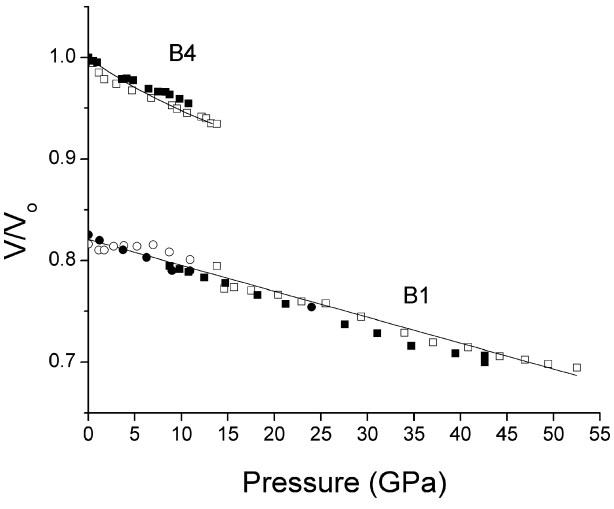

Figure 6 Compression curves for ZnO. Filled and open symbols represent data for bulk and the nanocrystals ZnO, respectively. Squares and circles denote data for increasing and decreasing pressures, respectively. Solid lines are Birch-Murnaghan equation of state of the B4 structure and the linear volume compressibility of the B1 structure in the nanocrystals.

occurs at transition pressures for both samples. This result indicates that the high-pressure ZnO B1 phase is not metallic, most likely still semiconductor, up to 18 GPa at ambient temperature. We further performed high-pressure optical measurements for bulk and the 12 nm ZnO samples. It is found that the B4-to-B1 transition for the 12 nm ZnO appears at around 14 ± 2 GPa while bulk ZnO has a transition at around 9 ± 1 GPa, in agreement with the data obtained from X-ray powder diffraction measurements. Our experimental data reveal that the transition pressure of the B4-to-B1 transformation in the ZnO system strongly depends on the grain size of ZnO crystals. The smaller the crystal, the higher the transition pressure.

3.2. Reduced transition pressure

Maghemite (γ-Fe_2O_3) has cubic symmetry with a structure that is closely related to the inverse spinel Fe_3O_4 (magnetite). At high pressure it transforms into hematite (α-Fe_2O_3) with corundum-type rhombohedral structure. We studied two γ-Fe_2O_3 samples with average grain sizes of 10 μm (hereafter called bulk) and 9 nm (hereafter called nano) using *in-situ* high-pressure X-ray powder diffraction with two pressure transmitting media: 16:3:1 methanol:ethanol:water solution and silicon oil [11]. Results obtained from both pressure media are the same. The measurements have shown that the transition pressure is 35 GPa for bulk and 27 GPa for 9 nm nanocrystals, having a 20% reduction of the transition pressure in the nanocrystals as compared with the bulk material. This is visualized by plotting the intensity ratio of the 311 and 220 peaks as a function of pressure, as shown in Fig. 7. The 311 line of the γ-Fe_2O_3 phase continues through the phase transition as the 110 line of the α-Fe_2O_3, whereas the 220 line of the γ-Fe_2O_3 phase has no counterpart in the α-Fe_2O_3 phase. Thus, the intensity ratio I(311)/I(220) approaches infinity at the transformation. It was also found that a 50% enhancement of the bulk

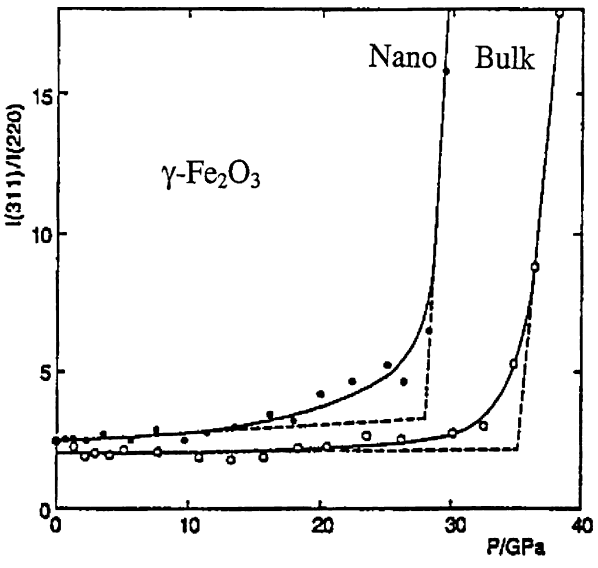

Figure 7 Intensity ratio $I_{\alpha\text{-Fe2O3}}(311)/I_{\gamma\text{-Fe2O3}}(220)$ vs. pressure for γ-Fe_2O_3. Filled circles denote nanocrystals and open circles denote bulk material.

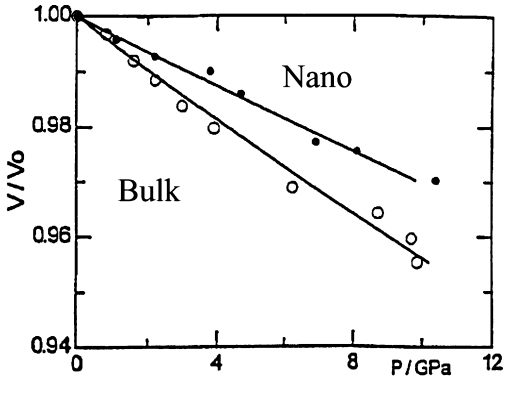

Figure 8 Compression curves for γ-Fe_2O_3 with the same notation as for Fig. 7. The full curves have been calculated from the Birch-Murnaghan equation.

modulus for nanocrystalline γ-Fe_2O_3 (305 ± 15 GPa) as compared with the bulk material (203 ± 10 GPa) in Fig. 8, whereas the bulk modulus is the same for bulk and nanocrystalline α-Fe_2O_3.

The reduction of transition pressure in nanocrystals as compared with bulk material has also been found in rutile-TiO_2. High-temperature/high-pressure X-ray diffraction in Fig. 9 has shown that the phase boundary between the rutile and α-PbO_2-type phases is shifted towards lower pressure for the nanocrystalline material as compared with bulk material [12]. Thus, for a given temperature, the transition pressure is lower for nanocrystalline material than for bulk TiO_2. In contrast, our recent measurements indicate that the low-pressure rutile structure is stable to pressures much higher than the bulk at room temperature.

Very recently, high-pressure Raman study on nanocrystalline CeO_2 was reported from Saxena's group [13]. They performed Raman spectroscopy measurements up to 36 GPa with and without pressure transmitting media. They found that the transition pressure of flurite-type-to orthorhombic $PbCl_2$-type phase transformation in CeO_2 nanocrystals is 26.5 GPa while it is at 32 GPa for bulk material. They further observed almost the same transition pressure in nanocrystalline CeO_2 compressed under quasihydrostatic and nonhydrostatic medium.

3.3. No change in transition pressure

It follows from above that the transition pressure may be enhanced as well as reduced in nanocrystalline material as compared with bulk material. We have also found systems where there is no change. Rutile-type tetragonal SnO_2 transforms into a fluorite-type cubic structure at high pressure. X-ray powder diffraction measurements show that the tetragonal-to-cubic transformation is sluggish [31]. Fig. 10 shows the intensity ratio $I_c(111)/I_t(110)$ vs. pressure for both bulk and nanocrystal SnO_2, where $I_c(111)$ and $I_t(110)$ are the peak intensities of the fluorite- and rutile-type phase, respectively. The rutile-to-cubic structure transformation in nanocrystals is sluggish with an onset transition pressure about 18 GPa. No significant difference in the onset transition pressure in bulk and nanocrystal SnO_2 (8 nm) was observed. This result was also confirmed by *in-situ* high-pressure electrical resistance measurements, as shown in Fig. 11. The sluggish rutile-to-cubic phase transformation in both bulk and nanocrystal SnO_2 is revealed by the gradual increase of electrical resistance above 18 GPa. Both rutile- and fluorite-type SnO_2 phases are semiconductors although the resistivity of the fluorite-type phase is larger than that of the rutile-type phase. Fig. 12 shows the pressure dependence of the relative volume for both bulk and nanocrystal SnO_2. The rutile-to-cubic phase transformation is accompanied by a volume collapse, $\Delta V = V^t - V^c$, with a relative volume change $\Delta V/V^t = 9.4\%$ at 18 GPa for both bulk and nanocrystal SnO_2.

The systems described above are all semiconductor compounds. We are also studying the element Fe and the alloy $Fe_{90}Cu_{10}$ produced by mechanically alloying [32]. Bcc α-Fe transforms into hcp ε-Fe at about 12 GPa, and this transition is widely used in the calibration of high-pressure cells. Our preliminary results indicate that the onset transition pressure is the same in bulk and nanocrystalline Fe as well as $Fe_{90}Cu_{10}$ nanocrystalline alloy, although the transformation kinetics seems to be very different.

4. Discussion

Phase transitions of the first order generally exhibit hysteresis. It manifests itself as a difference in the transition pressure in the forward and reveres directions in pressure-induced phase transitions in all systems reported here. The mechanism of pressure hysteresis is still poor understood. The lattice strain energy, caused by a discontinuous volume change at the transition, is often considered to be the main factor controlling the hysteresis. Based on simple considerations of the theory of elasticity, it has been shown that the strain energy is a function of the volume collapse at the transition. The low-pressure-to-high-pressure phase transformation associates a negative volume change. Thus, the

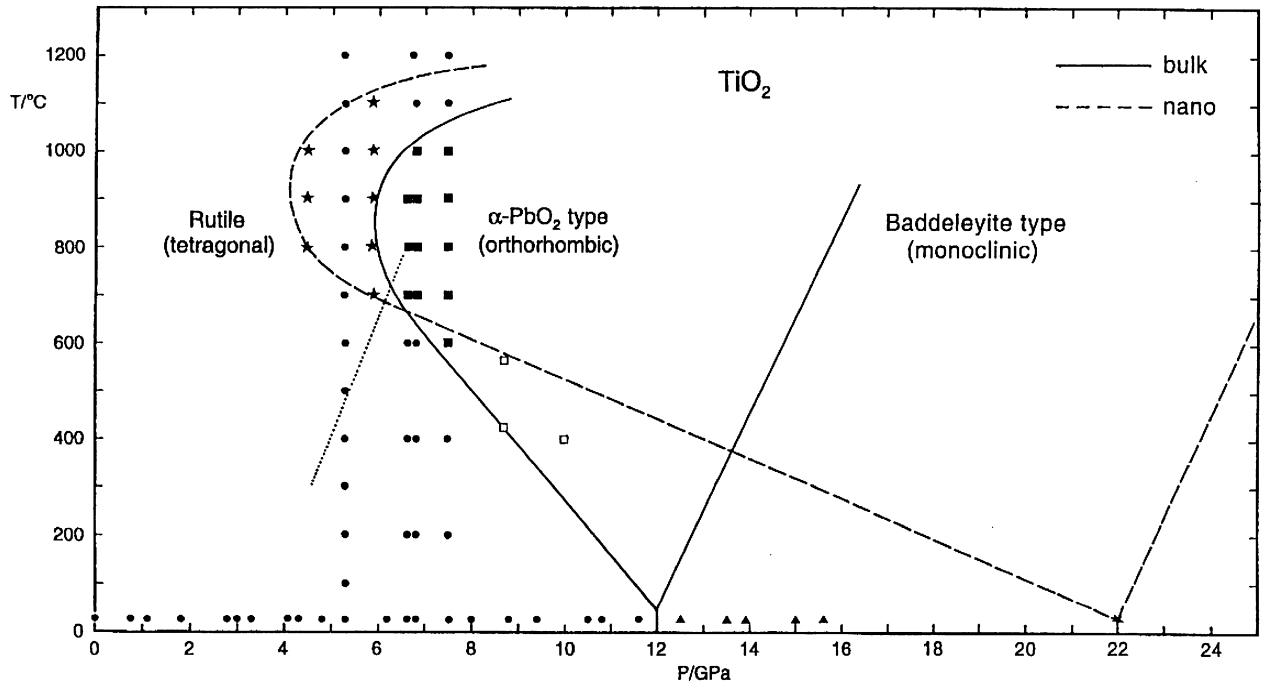

Figure 9 Phase diagram of TiO_2, obtained in heating and compression. Circles denote rutile; squares denote the α-PbO_2-type phase; triangles denote the baddeleyite-type phase. Open squares denote literature data: 8.7 GPa, 425 and 565°C [28]; 10 GPa, 400°C [29]. The α-PbO_2/ baddeleyite phase boundary (straight line, lower right-hand corner) has been calculated from Ref. [21]. The rutile/α-PbO_2 phase boundary is indicated by a curved full line for the bulk material and by a curved broken line for the nanocrystals, the stars denoting nanocrystals in the orthorhombic phase (for clarity, data points for the orthorhombic nanocrystals only are shown for pressures of 4.5 and 5.9 GPa). The dotted line indicates the rutile/α-PbO_2 phase boundary as reported by Akaogi *et al*. [39].

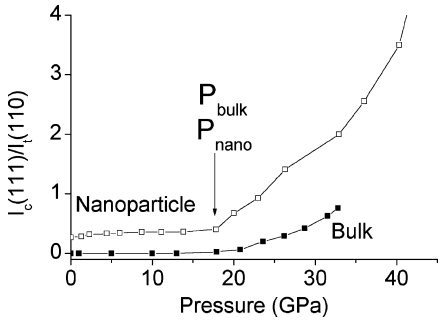

Figure 10 Intensity ratio $I_c(111)/I_t(110)$ vs. pressure for both bulk and nanocrystal SnO_2. The 111 line of the fluorite-type cubic phase and the 110 line of the rutile-type phase have no counterparts in the opposite phases. Thus, the intensity ratio, $I_c(111)/I_t(110)$, approaches infinity at the final stage of the transformation.

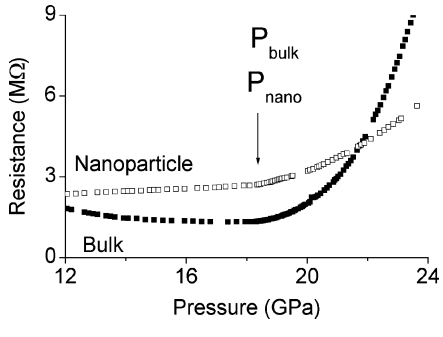

Figure 11 In-situ high-pressure electrical resistance for bulk and nanocrystal SnO_2 at ambient temperature.

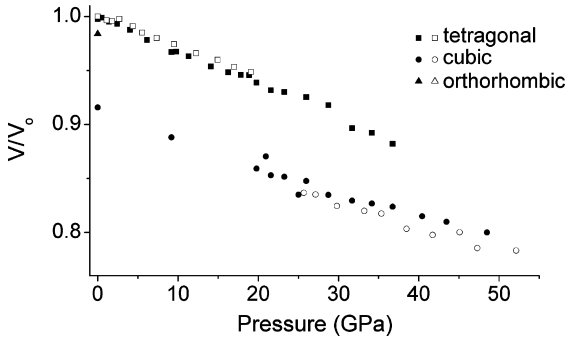

Figure 12 Volume per formula unit of SnO_2 as a function of pressure. The volumes have been normalized relative to V_o, the zero-pressure volume of the rutile-type phase. Filled and open symbols represent data for bulk and nanocrystal SnO_2, respectively.

nucleation of the high-pressure phase takes place under tension in the forward direction and under compression in the reverse direction. One would therefore expect the transition pressures to be different in the two directions. In the following section, we attempt to discuss possible contributions to the discrepancy of the upstroke transition pressures for both bulk and nanocrystalline materials.

The driving force of phase transformation is the reduction in Gibbs free energy, G, from the original (phase 1) to the final structure (phase 2). The definition of G per mole at constant pressure and temperature is $G = U + PV - TS$, where U is the internal energy per mole, P is the pressure, V is the volume per mole, T the absolute temperature and S the entropy per mole. For nanocrystals, the internal energy consists of contributions from the core, U_{ncore}, and the surface, U_{nsurf}. By the transformation from phase 1 to phase 2, the free energy changes for both bulk material at transition pressure P_B and nanocrystals at transition pressure P_n

can be expressed as

$$\begin{aligned}\Delta G_B(P_B) &= G_B(2, P_B) - G_B(1, P_B) \\ &= (U_B(2, P_B) - U_B(1, P_B)) + P_B(V_B(2, P_B) \\ &\quad - V_B(1, P_B)) - T(S_B(2) - S_B(1)), \qquad (1)\end{aligned}$$

$$\begin{aligned}\Delta G_n(P_n) &= G_n(2, P_n) - G_n(1, P_n) \\ &= (U_{ncore}(2, P_n) - U_{ncore}(1, P_n)) \\ &\quad + (U_{nsurf}(2, P_n) - U_{nsurf}(1, P_n)) \\ &\quad + P_n(V_n(2, P_n) - V_n(1, P_n)) \\ &\quad - T(S_n(2) - S_n(1)), \qquad (2)\end{aligned}$$

where B and n refer to bulk and nanocrystals, respectively. For simplicity, four assumptions are made: (1) In the transformation between solid crystalline phases at room temperature, the entropy change is assumed to be negligible; (2) The internal energy difference between phases for a given pressure is assumed to be the same for the bulk as for the core of the nanocrystals. This assumption is based on the experimental observation that many physical parameters for the core in nanocrystals are similar to the corresponding bulk materials [33], e.g., lattice parameters and co-ordination number; (3) The difference of strain energy induced at the transitions in both bulk and nanocrystalline materials is assumed to be negligible; and (4) The driving force, the difference of the free energies of phases 1 and 2, $\Delta G = G(1) - G(2)$, is assumed to be the same for both bulk and nanocrystalline samples at the transition pressures. (Note that the free energies of phases 1 and 2 could be not equal at the transition pressure.) Thus, the difference of transition pressures for both bulk and nanocrystals can be expressed by:

$$\begin{aligned}P_n - P_B &= P_B(\Delta V_B(P_B)/\Delta V_n(P_n) - 1) \\ &\quad + (U_{nsurf}(2, P_n) - U_{nsurf}(1, P_n))/\Delta V_n(P_n) \\ &\quad + ((U_B(1, P_B) - U_B(1, P_n)) - (U_B(2, P_B) \\ &\quad - U_B(2, P_n)))/\Delta V_n(P_n), \qquad (3)\end{aligned}$$

where the volume changes at the transition are $\Delta V_n(P_n) = V_n(1, P_n) - V_n(2, P_n)$ and $\Delta V_B(P_B) = V_B(1, P_B) - V_B(2, P_B)$. From Equation 3 it demonstrates that the transition pressure, P_n, depends on three components: (1) the volume changes for bulk and nanocrystals at the transitions, (hereafter Term1); (2) the surface energy difference between the phases involved, (hereafter Term2); and (3) the internal energy difference between the phases involved in bulk, (hereafter Term3). The last term can be calculated by the following integral: $U_B(i, P_B) - U_B(i, P_n) = -\int PdV$; $i = 1, 2$, using the experimental volume data as a function of pressure. Inserting all experimental data, P_n, P_B, $\Delta V_n(P_n)$, and $\Delta V_B(P_B)$, the surface energy difference, $U_{nsurf}(2, P_n) - U_{nsurf}(1, P_n)$ can be estimated. Assuming $U_{nsurf} = \gamma AN$, where γ is the average surface tension, A is the surface area of the crystal, and N the number of the crystal per mole, the difference of average surface tension between low- and high-pressure phase can be estimated. This could be a new method to determine the surface tension of materials. Equation 3 can be applied to uncover the major factor underlying the change of transition pressure in nanocrystals as compared with the corresponding bulk material. A few examples are given below.

(1) For the phase transition from the wurtzite (B4) to the rocksalt (B1) structure in 4.2 nm CdSe particles [4], it was reported that $P_n = 3.6$ GP, $P_B = 2$ GPa, with no difference of compressibility in both nanocrystal and bulk materials, indicating that the ratio of volume changes is close to unit, Term1 ≈ 0. Term2 and Term3 were estimated to be approximately 2 GPa and -0.4 GPa, respectively, from the reported experimental data. Then, the enhancement of the transition pressure in nanocrystals, P_n, is dominated by the surface energy difference. A similar explanation for the enhancement of transition pressure in nanocrystals was suggested by the authors [4]. The surface energy and average surface tension differences between B1 and B4 phases at the transition pressure is estimated to be $U_{nsurf}(B1) - U_{nsurf}(B4) = 6.2$ kJ/mol and $\gamma(B1) - \gamma(B4) = 0.13$ J/m^2 for 4.2 nm CdSe particles, respectively.

(2) For the B4-to-B1 phase transformation in 12 nm ZnO nanocrystals [8], inserting all experimental data into Equation 3, the surface energy difference, $U_{nsurf}(B1, P_n) - U_{nsurf}(B4, P_n)$, was estimated to be about 11 kJ/mol. The difference of average surface tension between phase B1 and B4 is estimated, $\gamma(B1)$–$\gamma(B4) = 1.5$ J/m^2. Using the reported data for $\gamma(B4)$, 0.3–0.7 J/m^2, in Ref. [34], the value of $\gamma(B1)$ is found for the first time to be $\gamma(B1) \approx 1.8$–2.2 J/m^2. Furthermore, from Equation 3 one can obtain Term1 = 0.47 GPa, Term2 = 5.2 GPa, Term3 = -0.48 GPa. It reveals that the surface energy difference at the transition is the dominating force, leading to the observed enhancement of the transition pressure for ZnO nanocrystals.

(3) For the phase transition of γ-to-α-Fe_2O_3 in 9 nm γ-Fe_2O_3 particles [11], it was found that $P_n = 27$ GPa; $P_B = 35$ GPa; Term1 = -14 GPa; Term2 = 4.7 GPa; Term3 = 1.3 GPa. Term2 and Term3 would favor an enhancement of the transition pressure for nanocrystals. However, the volume change for nanocrystals at the transition is approximately 65.8% larger than that for bulk. This dominates the reduction of the phase transition pressure in nanocrystals. The surface energy difference, $U_{nsurf}(\alpha\text{-}Fe_2O_3, P_n)$–$U_{nsurf}(\gamma\text{-}Fe_2O_3, P_n)$, was estimated to be about 18.5 kJ/mol and the difference of average surface tension between γ-Fe_2O_3 and α-Fe_2O_3 is estimated, $\gamma(\alpha\text{-}Fe_2O_3)$–$\gamma(\gamma\text{-}Fe_2O_3) = 0.84$ J/m^2. Using the reported data for $\gamma(\alpha\text{-}Fe_2O_3)$, 1.6–2 J/m^2, in Ref. [35], the value of $\gamma(\gamma\text{-}Fe_2O_3)$ is found to be 0.76–1.16 J/m^2, which is in good agreement with literature data, $\gamma(\gamma\text{-}Fe_2O_3) = 0.36$–$1.86$ J/m^2, reported in Ref. [36]. For the PbS system [7,10], due to the lack of experimental data, we can not analyze the main factor leading to the enhancement of the transition pressure in nanocrystals, as compared with bulk material. However, the volume collapse effect might be the main factor

because enhancement of compressibility with decreasing grain size was reported [7].

(4) For the rutile-to-fluorite-type phase transformation in SnO_2 [32], using the compression data in Fig. 12, it is found that Term1 and Term3 are small and close to zero. It reveals that the surface energy difference between rutile- and fluorite-type SnO_2 phase at the onset transition pressure, $P_n \approx P_B \approx 18$ GPa, could be very small. Thus, no significant difference in the onset transition pressure in nanocrystal SnO_2as compared with the corresponding bulk material could be explained by the small changes in the volume collapse, the surface energy difference, and the internal energy difference between the rutile- and fluorite-type phase at the transition.

5. Summaries

The nature of the change of transition pressure in nanocrystals as compared with the corresponding bulk material was addressed. We have shown that the grain-size effect on structural phase transition pressures can be of either sign, depending on the system under consideration. A thermodynamic analysis shows that the difference in transition pressure between nanocrystals and bulk material depends on three components: the ratio of volume collapses, the surface energy differences, and the internal energy differences. Whether there will be an enhanced, reduced or unchanged transition pressure depends on the relative importance of these three components.

Acknowledgments

I would like to acknowledge all of the members of my research group at Zhejiang University and Technical University of Denmark who contributed to the research presented here. I thank Hasylab in Hamburg, MAXlab in Lund, ESRF in Grenoble, and Spring8 in Japan for use of the synchrotron radiation facilities. Financial support from the National Natural Science Foundation of China (No. 50341032), Zhejiang University, the Danish Technical Research Council, the Danish Natural Sciences Research Council, and the EU programs "Improvement of Human Potential" and "Large Scale Facility" at the Bayerisches Geoinstitut is gratefully acknowledged.

References

1. See for example, "Nanophase Materials: Synthesis-Properties-Applications," edited by G. C. Hadjipanayis and R. W. Siegel (Kluwer Academic Publishers, Dordrecht, 1994) and "Fundamental Properties of Nanostructured Materials," edited by D. Fiorani and G. Sberveglieri (World Scientific, Singapore, 1994).
2. M. BRUCHEZ JR., M. MORONNE, P. GIN, S. WEISS and A. P. ALIVISATOS, *Science* **281** (1998) 2013.
3. W. C. W. CHAN and S. NIE, *ibid.* **281** (1998) 2016.
4. S. H. TOLBERT and A. P. ALIVISATOS, *ibid.* **265** (1994) 373.
5. *Idem.*, *J. Chem. Phys.* **102** (1995) 4642.
6. S. H. TOLBERT, A. B. HERHOLD, L. E. BRUS and A. P. ALIVISATOS, *Phys. Rev. Lett.* **76** (1996) 4385.
7. S. B. QADRI, J. YANG, B. R. RATNA, E. F. SKELTON and J. Z. HU, *Appl. Phys. Lett.* **69** (1996) 2205.
8. J. Z. JIANG, J. S. OLSEN, L. GERWARD, D. FROST, D. RUBIE and J. PEYRONNEAU, *Europhys. Lett.* **50** (2000) 48.
9. J. Z. JIANG, L. GERWARD, D. FROST, R. SECCO, J. PEYRONNEAU and J. S. OLSEN, *J. Appl. Phys.* **86** (1999) 6608.
10. J. Z. JIANG, L. GERWARD, R. SECCO, D. FROST, J. S. OLSEN and J. TRUCHENBRODT, *ibid.* **87** (2000) 2658.
11. J. Z. JIANG, J. STAUN OLSEN, L. GERWARD and S. MØRUP, *Europhys. Lett.* **44** (1998) 620.
12. J. STAUN OLSEN, L. GERWARD and J. Z. JIANG, *J. Phys. Chem. Solids* **60** (1999) 229.
13. A. REKHI, S. K. SAXENA and P. LAZOR, *J. Appl. Phys.* **89** (2001) 2968.
14. G. HUBER, K. SYASSEN and W. B. HOLZAPFEL, *Phys. Rev.* B **15** (1977) 5123.
15. H. K. MAO, P. M. BELL, J. W. SHANER and D. J. STEINBERG, *J. Appl. Phys.* **49** (1978) 3276.
16. F. BIRCH, *ibid.* **9** (1938) 279; *Phys. Rev.* **71** (1947) 809.
17. D. C. RUBIE, *Phase Transitions* **68** (1999) 431.
18. T. CHATTOPADHYAY, H. G. VON SCHNERING, W. A. GROSSHANS and W. B. HOLZAPFEL, *Physica* **139/140B** (1986) 356.
19. C. H. BATES, W. B. WHITE and R. ROY, *Science* **137** (1962) 993.
20. J. M. RECIO, R. PANDEY and V. LUANA, *Phys. Rev.* B **47** (1993) 3401.
21. J. E. JAFFE and A. C. HESS, *ibid.* **48** (1993) 7903.
22. L. GERWARD and J. STAUN OLSEN, *J. Synchrotron Radiat.* **2** (1995) 233.
23. H. KARZEL, W. POTZEL, M. KOFFERLEIN, W. SHIESSL, M. STEINER, U. HILLER, G. M. KALVIUS, D. W. MITCHELL, T. P. DAS, P. BLAHA, K. SCHWARZ and M. P. PASTERNAK, *Phys. Rev.* B **53** (1996) 11425.
24. M. WILSON and P. A. MADDEN, *Mol. Phys.* **90** (1997) 75.
25. J. M. RECIO, M. A. BLANCO, V. LUANA, R. PANDEY, L. GERWARD and J. STAUN OLSEN, *Phys. Rev.* B **58** (1998) 8949.
26. S. DESGRENIERS, *ibid.* **58** (1998) 14102.
27. E. YU. TONKOV (ed.), "High pressure Phase Transformations: A Handbook" (Gordon and Breach Science Publications, Philadephia, 1992) p. 624.
28. J. TANF and S. ENDO, in "High-Pressure Science and Technology," edited by S. C. Schmidt, J. W. Shaner, G. A. Samara and M. Ross (American Insitute of Physics, New York, 1994) p. 367.
29. J. C. JAMIESON and B. OLINGER, *Science* **161** (1968) 893.
30. M. AKAOGI, J. SUSAKI, T. YAGI, K. KUSABA, T. ATO, M. MATSUI and T. KIKEGAWA, in "The 30th High-Pressure Conference of Japan," edited by Y. Syono (Japan Society of High Pressure Science and Technology, Kyoto, 1989) p. 166.
31. J. Z. JIANG, L. GERWARD and J. STAUN OLSEN, *Scripta Mater.* **44** (2001) 1983.
32. *Idem.*, *Mater. Trans. JIM* **42** (2001) 1571.
33. H. GLEITER, *Progr. Mater. Sci.* **33** (1989) 223.
34. J. G. LI, *J. Mater. Sci. Lett.* **13** (1994) 400; and A. A. SOLOMON and F. HSU, *J. Amer. Ceramic. Soc.* **63** (1980) 467.
35. E. WASSERMAN, J. R. RUSTAD, A. R. FELMY and J. W. HALLEY, *Surf. Sci.* **385** (1997) 217.
36. A. CASARICO, P. CAVALLOTTI, D. COLOMBO, P. D'ARCANGELO, G. PETTENATI and P. G. VISIGALLI, *IEEE Trans. Magn.* **23** (1987) 86.

Received 11 September 2003
and accepted 27 February 2004